

# Circularly Polarized Wave Scattering from Two-Dimensional Dielectric Rough Sea Surface

Pengju Yang\*, Lixin Guo, and Qiang Wang

**Abstract**—Based on the polarimetric scattering model of second-order small-slope approximation (SSA-II) with tapered wave incidence under linear and circular polarization, monostatic and bistatic scattering from two-dimensional dielectric rough sea surface is investigated. The emphasis of the present study is on the polarization signature of the scattered wave under circularly polarized wave incidence, which is related to the Brewster angle. Numerical simulations show that for bistatic configuration under circularly polarized wave incidence, the polarization state of scattering wave strongly depends on incident angle, scattering angle, as well as their relation to the Brewster angle associated with medium permittivity.

## 1. INTRODUCTION

Global Positioning System (GPS) signal scattering from rough sea surface has received considerable attention due to its extensive applications in ocean remote sensing [1–4], which transmits right-hand circularly polarized (RHCP) wave at L-band. Due to the expected phase shift at reflection, the reflected GPS signal near the specular direction is left-hand circularly polarized (LHCP) wave. However, the data collected in the experiments show that a strong RHCP component is also present [5]. Hence, the determination of polarization state of GPS signal scattered wave from rough sea surface is crucially important for choosing the polarization channel of GPS receiver. The investigation of circularly polarized wave scattering from 2-D rough surface requires the calculation of fully polarimetric scattering including co-polarization ( $HH$ ,  $VV$ ) and cross-polarization ( $HV$ ,  $VH$ ) scattering, which is a three-dimensional (3-D) electrically large problem and is beyond the capability of numerical methods such as method of moments (MoM) [6–9], finite-difference time-domain (FDTD) [10, 11], etc. Analytical approximate models can deal with 3-D electrically large problem but are limited by their validity domains. Moreover, most of the analytical approximate models cannot correctly predict the depolarized scattering from rough surface. Among the analytical approximate models, the Kirchhoff approximation (KA) [12–14] also known as the physical optics or the tangent plane approximation cannot correctly show distinct polarization dependence. The second-order small perturbation method (SPM) [15–17] can predict the depolarized scattering in and out the plane of incidence, but its validity domain is restricted to the small roughness cases. The two scale model (TSM) [18–21] also known as composite surface model underestimates the cross-polarized components due to the neglect of second-order Bragg scattering. In comparison with the classical model such as SPM, KA and TSM, the modern analytical approximate model of second-order small-slope approximation (SSA-II) takes into account the mutual transformation of the two linear polarization states caused by facets tilts as well as the second-order Bragg scattering [22], and thus can predict the depolarized scattering from rough sea surface both in and outside the plane of incidence.

---

*Received 7 September 2015, Accepted 3 November 2015, Scheduled 6 November 2015*

\* Corresponding author: Peng-Ju Yang (pjyang@yeah.net).

The authors are with the School of Physics and Optoelectronic Engineering, Xidian University, Xi'an 710071, China.

In [23], the integral equation method (IEM) has been used to predict the polarization properties of GPS signal scattered from a wind-driven ocean, in which the polarization dependence on the Brewster effect is not taken into account, however. As we know, for RHCP wave incident upon smooth dielectric half-space from vacuum, the polarization state of reflected field is LHCP and RHCP wave for incident angle smaller and larger than the Brewster angle, respectively. On the other hand, for rough surface under vertical-polarized wave incidence, investigations have demonstrated that the Brewster effect was also present for certain incident angles, at which the reflectivity takes minimum value instead of null, and that the Brewster angle exhibited a small negative shift with increasing roughness [24]. The present study was motivated by the speculation that the polarization states of GPS signal scattered wave from rough sea surface might be sensitive to the Brewster angle as well as configuration angles. Consequently, based on the fully polarimetric scattering model of SSA-II, the present study is devoted mainly to the analysis of the polarization state of scattered wave under circularly polarized wave incidence with emphasis on the polarization dependence of scattered wave on the Brewster effect.

## 2. CIRCULARLY POLARIZED WAVE SCATTERING MODELING BASED ON SSA-II WITH TAPERED WAVE INCIDENCE

The small-slope approximation (SSA) [25] theory consists of a basic approximation of the theory (SSA-I) and second-order corrections to it (SSA-II) and represents a systematic expansion of a scattering amplitude with respect to slopes of rough surface, which has been successfully applied to evaluate microwave scattering from rough sea surfaces [22, 26]. Although SSA-I is much more efficient than SSA-II, it cannot predict the depolarization of wave scattering from rough surfaces in the plane of incidence. Thus, in this paper, the SSA-II model instead of SSA-I is used to evaluate the linearly and circularly polarized wave scattering from two-dimensional (2-D) dielectric rough sea surface.

The geometry of electromagnetic scattering from 2-D sea surface is illustrated in Fig. 1. The configuration angles  $(\theta_i, \varphi_i, \theta_s, \varphi_s)$  represent incident angle, incident azimuth angle, scattering angle, and scattering azimuth angle, respectively.  $\bar{k}_i = (\bar{k}_0, q_0)$  and  $\bar{k}_s = (\bar{k}, q)$  are the incident wave vector and scattering wave vector, respectively.

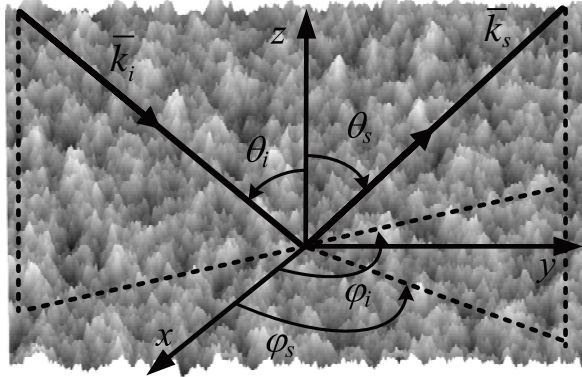


**Figure 1.** Geometry of the 2-D sea surface scattering problem.

In this paper, a tapered plane wave is chosen as the incident field to reduce the edge effect caused by the limited surface size of  $L_x \times L_y$ , and the tapered incident wave can be expressed as [27]

$$\bar{E}_i(\bar{r}) = T(\bar{r}) \exp(i\bar{k}_i \cdot \bar{r}) \quad (1)$$

$$T(\bar{r}) = \exp[i(\bar{k}_i \cdot \bar{r})w] \exp(-t_x - t_y) \quad (2)$$

where

$$t_x = \frac{(x \cos \theta_i \cos \varphi_i + y \cos \theta_i \sin \varphi_i + z \sin \theta_i)^2}{g^2 \cos^2 \theta_i} \quad (3)$$

$$t_y = \frac{(-x \sin \varphi_i + y \cos \varphi_i)^2}{g^2} \quad (4)$$

$$w = \frac{1}{k_i^2} \left( \frac{2t_x - 1}{g^2 \cos^2 \theta_i} + \frac{2t_y - 1}{g^2} \right) \quad (5)$$

and  $g$  is the parameter that controls the tapering of the incident wave. Thus, the original scattering amplitude of the SSA-II model can be expressed as follows after introducing the tapered incident wave

$$S(\bar{k}, \bar{k}_0) = \frac{2\sqrt{q_0 q}}{(q_0 + q)\sqrt{P_{inc}}} \int \frac{d\bar{r}}{(2\pi)^2} T(\bar{r}) \times \exp[-i(\bar{k} - \bar{k}_0) \cdot \bar{r} + i(q + q_0)h(\bar{r})] \\ \times \left( B(\bar{k}, \bar{k}_0) - \frac{i}{4} \int M(\bar{k}, \bar{k}_0; \bar{\xi}) h(\bar{\xi}) \times \exp(i\bar{\xi} \cdot \bar{r}) d\bar{\xi} \right) \quad (6)$$

where  $P_{inc}$  is the incident wave power captured by the sea surface of limited size and

$$h(\bar{\xi}) = \frac{1}{(2\pi)^2} \int h(\bar{r}) \exp(-i\bar{\xi} \cdot \bar{r}) d\bar{r} \quad (7)$$

is the Fourier transformation of the surface elevation  $h(\bar{r})$ . The term  $\frac{i}{4} \int M(\bar{k}, \bar{k}_0; \bar{\xi}) h(\bar{\xi}) \times \exp(i\bar{\xi} \cdot \bar{r}) d\bar{\xi}$  denotes the second-order correction to the first-order small slope approximation, and (6) corresponds to first-order small slope approximation by using  $M(\bar{k}, \bar{k}_0; \bar{\xi}) = 0$ . It can be proven that in a general case  $M(\bar{k}, \bar{k}_0; 0) = 0$ , and for this reason the term associated with  $M(\bar{k}, \bar{k}_0; \bar{\xi})$  in (6) is, in fact, proportional to the slopes of the rough surface rather than the elevations themselves.  $M(\bar{k}, \bar{k}_0; \bar{\xi})$  describes a contribution from the second-order Bragg scattering process and is related to the Bragg kernel  $B$  and  $B_2$  by

$$M(\bar{k}, \bar{k}_0; \bar{\xi}) = B_2(\bar{k}, \bar{k}_0; \bar{k} - \bar{\xi}) + B_2(\bar{k}, \bar{k}_0; \bar{k} + \bar{\xi}) + 2(q_0 + q)B(\bar{k}, \bar{k}_0) \quad (8)$$

where the kernel functions of  $B$  and  $B_2$  are  $2 \times 2$  matrices describing mutual transformations of the EM waves of different polarizations, which depend mainly on the polarizations, configuration angles, and the permittivity of the lower medium. The detailed derivation and corresponding kernel functions of the SSA model can be found in [25].

The scattering matrix  $S_c$  in the basis of circularly polarized waves is related to the scattering matrix  $S$  for linearly polarized waves by the following unitary transformation [25]

$$S_c = \begin{bmatrix} S_{RR} & S_{RL} \\ S_{LR} & S_{LL} \end{bmatrix} = \frac{1}{2} \begin{bmatrix} 1 & i \\ 1 & -i \end{bmatrix} S \begin{bmatrix} 1 & 1 \\ -i & i \end{bmatrix} \quad (9)$$

By a simple matrix manipulation, the left-hand and right-hand polarized wave scattering amplitude under RHCP wave incidence is expressed as

$$S_{LR} = (S_{vv} - S_{hh} - iS_{vh} - iS_{hv})/2 \quad (10)$$

$$S_{RR} = (S_{vv} + S_{hh} - iS_{vh} + iS_{hv})/2 \quad (11)$$

where  $S_{vv}$ ,  $S_{hh}$ ,  $S_{vh}$ , and  $S_{hv}$  are scattering amplitude for linearly polarized waves. The first subscript of scattering amplitude  $S$  denotes the polarization state of scattered wave, whereas the second subscript represents the polarization state of incident wave. For example, index LR means that the polarization state of scattered and incident field is LHCP and RHCP wave, respectively. It should be noted that the scattering amplitude of circularly polarized wave takes into account both co-polarized and cross-polarized components.

Based on the scattering amplitude calculated from small slope approximation, the scattering coefficient for both linear and circularly polarized wave is defined as

$$\sigma = 4\pi q_0 q \left\langle |S_{pq}(\bar{k}, \bar{k}_0)|^2 \right\rangle \quad (12)$$

where the angular bracket  $\langle \cdot \rangle$  denotes the ensemble average over sea surface realizations.  $S_{pq}$  is scattering amplitude for linearly or circularly polarized waves, in which subscripts  $p$  and  $q$  are polarizations and can be either  $h$ ,  $v$ ,  $R$  or  $L$ .

For smooth surface under circularly polarized wave incidence, the reflected wave can be analytically determined. In fact, under RHCP wave incidence on smooth plane from vacuum, the polarization state

of reflected field is LHCP and RHCP wave for incident angle smaller and larger than the Brewster angle, respectively. Strictly speaking, the polarization state of reflected field is elliptically polarized with LHCP or RHCP wave dominating. Under circularly polarized wave incidence, the polarization signature of the scattered wave from rough sea surface is more sophisticated. In what follows, the SSA-II model is utilized for calculating the angular distribution of the scattered waves at different polarizations. In the following simulation section, we will show that for bistatic configuration under circularly polarized wave incidence, the polarization signature of the scattered wave depends strongly on the incident angle, scattering angle as well as their relation to the Brewster angle.

### 3. NUMERICAL RESULTS AND DISCUSSION

In the following simulations, the radar frequency is 1.2 GHz. The relative complex permittivity of sea surface is  $\epsilon_r = 73.2 + i67.2$  at salinity of 30 parts per thousand and sea water temperature of 20°C in terms of Debye expression. The surface size is  $L_x = L_y = 64$  m and the sampling interval is  $\lambda/8$  with  $\lambda$  being electromagnetic wavelength. The tapering parameter  $g$  is set to be  $L_x/4$  to reduce the edge effect caused by the limited surface size. The sea surface roughness spectrum proposed by Elfouhaily et al. combined with the spectral method is used in the present study for generating rough sea surface. The wind fetch involved in Elfouhaily et al. spectrum [28] is fixed at 30 km. The final monostatic and bistatic scattering is an ensemble average over 100 sea surface realizations. In all simulations, the radar is looking upwind.

Figures 2(a) and (b) present the backscattering coefficient of linearly and circularly polarized wave scattered from 2-D sea surface with wind speed  $U_{10} = 3$  m/s and  $U_{10} = 5$  m/s, respectively. Obviously, the co-polarized scattering intensity is much stronger than the cross-polarized one except for larger incident angles. This is attributed to the fact that the rough sea surface backscattering is dominated by the co-polarized scattering process. Moreover, as the incident angle increases, the backscattering coefficient for  $VV$  polarization is larger than that for  $HH$  polarization. This is due to the fact that a Bragg scattering component is stronger for  $VV$  polarization than for  $HH$  polarization, and that the scattering at small incident angles is dominated by specular reflections and Bragg scattering becomes dominant as incident angle increases. Also, it is very interesting to observe that  $HV$ -polarized backscattering coefficient is equal to  $VH$ -polarized one. This arises from the reciprocity which means that  $HV$ -polarized backscattering is equal to  $VH$ -polarized backscattering. On the other hand, the reciprocity of cross-polarized backscattering demonstrates the validity of SSA-II model. As for RHCP incident wave, the LR-polarized backscattering coefficient is much stronger than the LR-polarized one within small and moderate incident angle domains, and they eventually coincide with each other with incident angle increasing. This means that, for RHCP incidence wave, the backscattered power is dominated by LHCP wave.

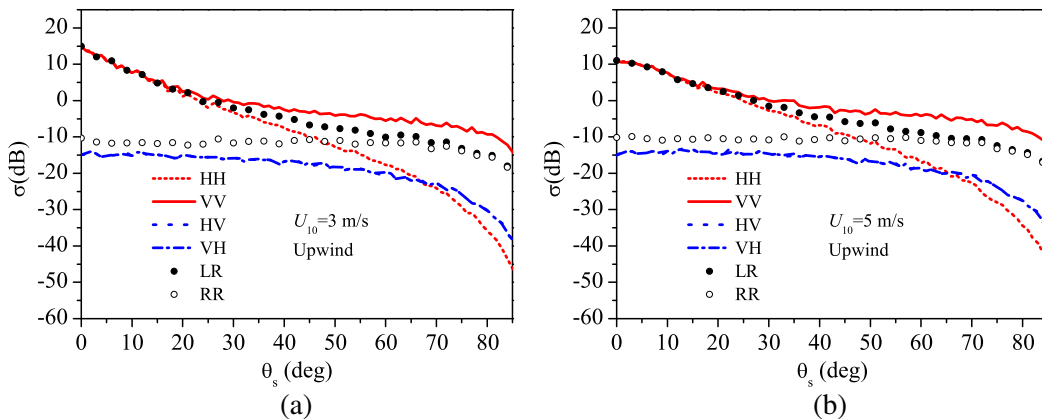


**Figure 2.** Comparison of linearly and circularly polarized backscattering coefficient.

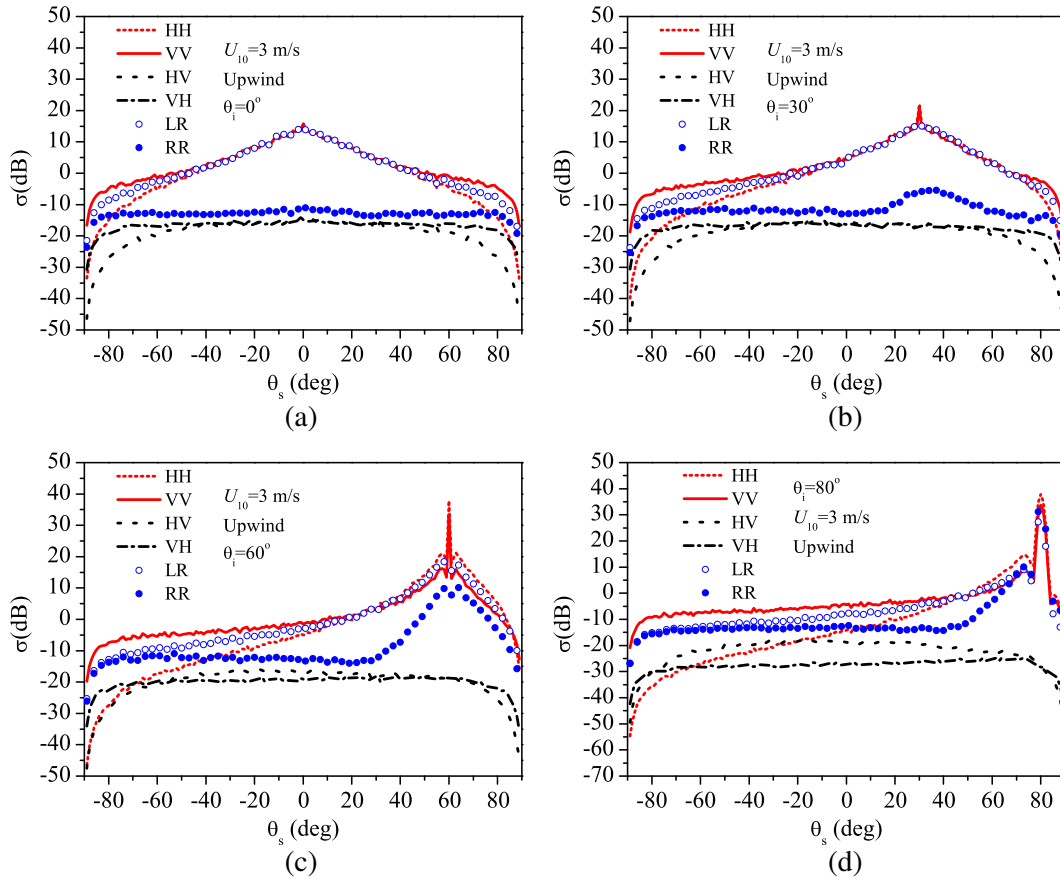


**Figure 3.** Comparison of linearly and circularly polarized bistatic scattering coefficient within the plane of incidence. (a)  $\theta_i = 0^\circ$ , (b)  $\theta_i = 30^\circ$ , (c)  $\theta_i = 60^\circ$ , (d)  $\theta_i = 80^\circ$ .

Figures 3(a), (b), (c) and (d) exhibit the bistatic scattering coefficient of linearly and circularly polarized wave within the plane of incidence for incident angle  $\theta_i = 0^\circ$ ,  $\theta_i = 30^\circ$ ,  $\theta_i = 60^\circ$  and  $\theta_i = 80^\circ$ , respectively. The wind speed is  $U_{10} = 3$  m/s. Due to a strong coherent scattering in the specular direction, obvious peaks appear for both co-polarized and circularly polarized scattering coefficient as depicted in Fig. 3. In the case of linear polarization, we can readily observe that the co-polarized scattering intensity is significantly stronger than the cross-polarized one in the vicinity of the specular direction, whereas their difference is relatively small far away from the specular direction. We attribute this phenomenon to the fact that the sea surface bistatic scattering is dominated by the co-polarized rather than the cross-polarized scattering process for almost all the scattering angle domains in the case of linear polarization. For circularly polarized incident wave under small incident angle  $\theta_i = 0^\circ$  and  $\theta_i = 30^\circ$ , the LR-polarized scattering wave is predominant regardless of scattering angle as depicted in Figs. 3(a) and (b). This means that, the polarization state of incident wave has changed from RHCP to LHCP due to the phase shift of scattering wave, which is similar to the phase shift of Fresnel reflection coefficient for smooth infinite half-space. More specifically, under RHCP wave incidence on smooth surface from vacuum, the reflected field is purely LHCP wave when incident angle is smaller than the Brewster angle associated with medium permittivity. Strictly speaking, the reflected field is elliptically polarized wave with LHCP wave dominating. It is also interesting to note that the reflected wave is linearly polarized for incident angle equal to the Brewster angle due to the Brewster effect, in which the reflectivity at vertical polarization goes to zero. For circularly polarized incident wave under larger incident angle  $\theta_i = 60^\circ$  and  $\theta_i = 80^\circ$ , we can observe a strong RR-polarized wave component for larger scattering angles as depicted in Figs. 3(c) and (d). Moreover, it is interesting to observe that for larger incident angle  $\theta_i = 80^\circ$ , the RR-polarized scattering wave component becomes comparable to or

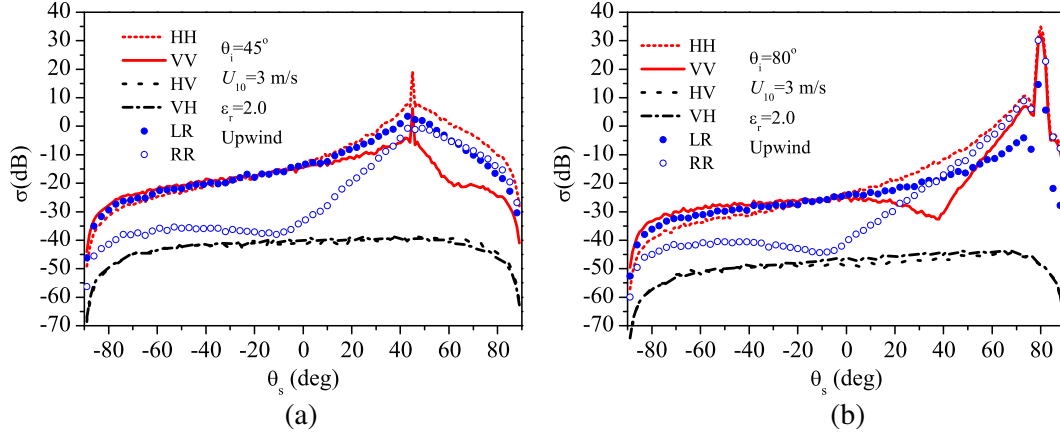


**Figure 4.** Bistatic scattering coefficient versus scattering angle within the plane of incidence under linear and circular polarization wave incidence with assumption  $\varepsilon_r = 2.0$ . (a)  $\theta_i = 45^\circ$ , (b)  $\theta_i = 80^\circ$ .

even larger than the LR-polarized one for larger scattering angles as depicted in Fig. 3(d). Comparing Figs. 3(a) and (b) with (c) and (d), we can find that the incidence angles are much closer to the large Brewster angle arising from the large permittivity of sea surface for the latter case than for the former case. Hence, we can speculate that the polarization state of the scattered wave under circularly polarized wave incidence depends strongly on the incident angle, scattering angle, as well as the Brewster angle associated with medium permittivity.

Due to the large dielectric constant of sea water, the Brewster angle at vertical polarization is very large. It is not easy to observe the Brewster effect for rough sea surface and its relation to the polarization signature of scattering wave from rough sea surface under circularly polarized wave incidence. Thus, to better show the polarization dependence of scattering wave on the Brewster effect, we perform additional calculations under assumption  $\varepsilon_r = 2.0$  in Figs. 4(a) and (b) for incident angle  $\theta_i = 45^\circ$  and  $\theta_i = 80^\circ$ , respectively. For permittivity  $\varepsilon_r = 2.0$  under vertical polarization, the Brewster angle for smooth surface is  $\theta_B = \tan^{-1}(\sqrt{\varepsilon_r}) \approx 54.7^\circ$ . In Figs. 4(a) and (b), we can readily observe that the LR-polarized scattering intensity is first larger than the RR-polarized one. As scattering angle increases, the LR-polarized scattering intensity becomes equal to the RR-polarized one in the vicinity of the scattering angle  $60^\circ$  and  $40^\circ$  as in Figs. 4(a) and (b), respectively. The angle  $60^\circ$  and  $40^\circ$  are corresponding to the angle of a minimum reflectivity at vertical polarization for rough surface as depicted in Figs. 4(a) and (b), respectively. Especially in Fig. 4(b), an obvious minimum reflectivity at vertical polarization for rough surface can be observed. For scattering angle larger than the angle of a minimum reflectivity at vertical polarization for rough surface, the RR-polarized scattering intensity becomes comparable to or even larger than the LR-polarized one. In Fig. 4(a), although the incident angle is smaller than (but close to) the Brewster angle, it is interesting to observe that for scattering angle smaller than (but close to) the Brewster angle  $\theta_B \approx 54.7^\circ$  a strong RR-polarized wave component can be observed due to sea surface roughness, which is comparable to the LR-polarized wave component. It is also indicated that for scattering angle larger than the Brewster angle, the RR-polarized wave component is even larger than the LR-polarized one as depicted in Fig. 4(a). In fact, under RHCP wave incidence on flat dielectric surface from vacuum, there exists no RR-polarized wave component and the reflected field is purely LHCP wave for incident angle smaller than the Brewster angle. In Fig. 4(b), it is observed that the angle of an obvious minimum reflectivity at vertical polarization is smaller than the Brewster angle  $\theta_B \approx 54.7^\circ$ . This is due to the shift in Brewster angle at vertical polarization for rough surface, in which the location of the angle of a minimum reflectivity at vertical polarization for rough surface exhibits a shift towards decreasing angle of incidence. In comparison with smooth surface, the reflectivity for rough surface at vertical polarization no longer goes to zero at some angle of incidence. Instead, it goes through a minimum at certain incident angle, which is close to and generally smaller than the Brewster angle given by equation  $\theta_B = \tan^{-1}\sqrt{\varepsilon_r}$ . Moreover, the angle of a minimum reflectivity at vertical polarization for rough surface is generally smaller than the Brewster for smooth surface [24, 29, 30].

#### 4. CONCLUSION

In this paper, electromagnetic scattering from 2-D rough sea surface under linear and circular polarization wave incidence has been investigated. The numerical results show that for linearly polarized incident wave, both monostatic and bistatic scatterings are dominated by co-polarized rather than cross-polarized scattering process. Under RHCP wave incidence, the LHCP scattered wave is predominant for backscattering case. For bistatic configuration under RHCP wave incidence, the polarization state of scattering wave depends strongly on configuration angles and the Brewster angle associated with medium permittivity. More specifically, the scattering field is dominated by LHCP wave for incident angle much smaller than the Brewster angle regardless of scattering angle. However, for both incident and scattering angle closer to or larger than the Brewster angle, the RHCP wave becomes comparable to or even larger than LHCP wave. These qualitative results of the scattering wave polarization state under circularly polarized wave incidence are potentially valuable for choosing the polarization channel of GPS receiver.

#### ACKNOWLEDGMENT

This work was supported by the National Science Foundation for Distinguished Young Scholars of China (Grant No. 61225002) and the Scientific Research Program Funded by Shaanxi Provincial Education Department (No. 15JK1180).

#### REFERENCES

1. Garrison, J. L., A. Komjathy, V. U. Zavorotny, and S. J. Katzberg, "Wind speed measurement using forward scattered GPS signals," *IEEE Trans. Geosci. Remote Sensing*, Vol. 40, No. 1, 50–65, 2002.
2. Komjathy, A., V. U. Zavorotny, P. Axelrad, G. H. Born, and J. L. Garrison, "GPS signal scattering from sea surface: Wind speed retrieval using experimental data and theoretical model," *Remote Sens. Environ.*, Vol. 73, No. 2, 162–174, 2000.
3. Rius, A., J. M. Aparicio, E. Cardellach, M. Martín-Neira, and B. Chapron, "Sea surface state measured using GPS reflected signals," *Geophys. Res. Lett.*, Vol. 29, No. 23, 2122, 2002.
4. Zavorotny, V. U. and A. G. Voronovich, "Scattering of GPS signals from the ocean with wind remote sensing application," *IEEE Trans. Geosci. Remote Sensing*, Vol. 38, No. 2, 951–964, 2000.
5. Thompson, D. R., T. M. Elfouhaily, and J. L. Garrison, "An improved geometrical optics model for bistatic GPS scattering from the ocean surface," *IEEE Trans. Geosci. Remote Sensing*, Vol. 43, No. 12, 2810–2821, 2005.
6. Barzegar-Parizi, S. and A. A. Shishegar, "Electromagnetic wave scattering analysis from 2-D periodic rough surfaces using complex images technique," *IEEE Trans. Geosci. Remote Sensing*, Vol. 53, No. 2, 862–868, 2015.
7. Brennan, C., D. Trinh-Xuan, M. Mullen, P. Bradley, and M. Condon, "Improved forward backward method with spectral acceleration for scattering from randomly rough lossy surfaces," *IEEE Trans. Antennas Propag.*, Vol. 61, No. 7, 3922–3926, 2013.
8. Luo, H. J., G. D. Yang, Y. H. Wang, J. C. Shi, and Y. Du, "Numerical studies of sea surface scattering with the GMRES-RP method," *IEEE Trans. Geosci. Remote Sensing*, Vol. 52, No. 4, 2064–2073, 2014.
9. Miret, D., G. Soriano, and M. Saillard, "Rigorous simulations of microwave scattering from finite conductivity two-dimensional sea surfaces at low grazing angles," *IEEE Trans. Geosci. Remote Sensing*, Vol. 52, No. 6, 3150–3158, 2014.
10. Jia, C. G., L. X. Guo, and P. J. Yang, "EM scattering from a target above a 1-D randomly rough sea surface using GPU-based parallel FDTD," *IEEE Antennas Wirel. Propag. Lett.*, Vol. 14, 217–220, 2015.

11. Kuang, L. and Y. Q. Jin, "Bistatic scattering from a three-dimensional object over a randomly rough surface using the FDTD algorithm," *IEEE Trans. Antennas Propag.*, Vol. 55, No. 8, 2302–2312, 2007.
12. Fung, A. K. and H. J. Eom, "Multiple scattering and depolarization by a randomly rough Kirchhoff surface," *IEEE Trans. Antennas Propag.*, Vol. 29, No. 3, 463–471, 1981.
13. Tsang, L. and J. A. Kong, *Scattering of Electromagnetic Waves: Advanced Topics*, Vol. 3, Wiley-Interscience, New York, 2001.
14. Ulaby, F. T., R. K. Moore, and A. K. Fung, *Microwave Remote Sensing: Active and Passive. Volume II: Radar Remote Sensing and Surface Scattering and Emission Theory*, Vol. 2, Addison-Wesley, Massachusetts, 1982.
15. Johnson, J. T., "Third-order small-perturbation method for scattering from dielectric rough surfaces," *J. Opt. Soc. Am. A*, Vol. 16, No. 11, 2720–2736, 1999.
16. Nieto-Vesperinas, M., "Depolarization of electromagnetic waves scattered from slightly rough random surfaces: A study by means of the extinction theorem," *J. Opt. Soc. Am.*, Vol. 72, No. 5, 539–547, 1982.
17. Valenzuela, G. R., "Depolarization of EM waves by slightly rough surfaces," *IEEE Trans. Antennas Propag.*, Vol. 15, No. 4, 552–557, 1967.
18. Bass, F. G., I. M. Fuks, A. I. Kalmykov, I. E. Ostrovsky, and A. D. Rosenberg, "Very high frequency radiowave scattering by a disturbed sea surface. Part II: Scattering from an actual sea surface," *IEEE Trans. Antennas Propag.*, Vol. 16, No. 5, 560–568, 1968.
19. Fung, A. K. and H. L. Chan, "Backscattering of waves by composite rough surfaces," *IEEE Trans. Antennas Propag.*, Vol. 17, No. 5, 590–597, 1969.
20. Luo, H. and Y. Du, "Comparison of the two-scale and three-scale models for bistatic electromagnetic scattering from ocean surfaces," *Progress In Electromagnetics Research*, Vol. 138, 519–536, 2013.
21. Plant, W. J., "A two-scale model of short wind-generated waves and scatterometry," *J. Geophys. Res.*, Vol. 91, No. C9, 10735–10749, 1986.
22. Voronovich, A. G. and V. U. Zavorotny, "Full-polarization modeling of monostatic and bistatic radar scattering from a rough sea surface," *IEEE Trans. Antennas Propag.*, Vol. 62, No. 3, 1362–1371, 2014.
23. Zuffada, C., A. Fung, J. Parker, M. Okolicanyi, and E. Huang, "Polarization properties of the GPS signal scattered off a wind-driven ocean," *IEEE Trans. Antennas Propag.*, Vol. 52, No. 1, 172–188, 2004.
24. Maradudin, A. A., R. E. Luna, and E. R. Méndez, "The Brewster effect for a one-dimensional random surface," *Waves in Random Media*, Vol. 3, No. 1, 51–60, 1993.
25. Voronovich, A. G., *Wave Scattering from Rough Surfaces*, 2nd Edition, Springer-Verlag, Berlin, 1999.
26. Nie, D., M. Zhang, and N. Li, "Investigation on microwave polarimetric scattering from two-dimensional wind fetch- and water depth-limited nearshore sea surfaces," *Progress In Electromagnetics Research*, Vol. 145, 251–261, 2014.
27. Tsang, L., J. A. Kong, K. H. Ding, and C. O. Ao, *Scattering of Electromagnetic Waves: Numerical Simulations*, Vol. 2, Wiley-Interscience, New York, 2001.
28. Elfouhaily, T., B. Chapron, K. Katsaros, and D. Vandemark, "A unified directional spectrum for long and short wind-driven waves," *J. Geophys. Res.*, Vol. 102, No. C7, 15781–15796, 1997.
29. Greffet, J. J., "Theoretical model of the shift of the Brewster angle on a rough surface," *Opt. Lett.*, Vol. 17, No. 4, 238–240, 1992.
30. Saillard, M. and D. Maystre, "Scattering from metallic and dielectric rough surfaces," *J. Opt. Soc. Am. A*, Vol. 7, No. 6, 982–990, 1990.